Wavelength-dependent neutron depolarization studies of the domain structure in ferromagnetic amorphous alloys

1993 J. Phys.: Condens. Matter 5 9277

(http://iopscience.iop.org/0953-8984/5/50/009)

J. Phys.: Condens. Matter 5 (1993) 9277–9286. Printed in the UK

Wavelength-dependent neutron depolarization studies of the domain structure in ferromagnetic amorphous alloys

K Krezhov†, V Lilkov†, P Konstantinov† and D Korneev‡

† Institute of Nuclear Research and Nuclear Energy, Bulgarian Academy of Sciences, 72 Tsarigradsko Chaussee Boulevard, Sofia 1784, Bulgaria

‡ Frank Laboratory of Neutron Physics, Joint Institute of Nuclear Research at Dubna, Moscow Region, Russia

Received 10 August 1993, in final form 8 October 1993

Abstract. The feasibility of using the wavelength-dependent neutron depolarization method for bulk domain structure studies is demonstrated using pulsed polarized neutrons. Information on the mean magnetization, static magnetization fluctuations, and magnetic anisotropy was obtained for an amorphous ferromagnetic ribbon of $Fe_{78}Co_{8.1}B_{13.9}$ taken as an example. Several domain models were tested. A simple model of penetrating domains was found to be reasonable for as-cast ribbon under favourable circumstances.

1. Introduction

The actual domain structure is usually studied by means of the Bitter method, magneto-optical Kerr effect, and electron microscopy (SEM and TEM). The information obtained is related to the surface, or at least the surface state strongly influences the domain pattern. Less is known about the possibilities offered by the neutron depolarization technique to get results concerning the bulk, although several studies have been published. Rekveldt and his collaborators (see [1, 2], and references therein) have applied a full three-dimensional analysis of the polarization state of a polarized monochromatic neutron beam before and after transmission through the material. The present paper deals with the possibilities for domain structure description by analysing the wavelength dependence of the depolarization of a polychromatic beam of polarized neutrons. Results on specimens of amorphous $Fe_{78}Co_{8.1}B_{13.9}$ ribbon are presented here as an example. The neutron time-of-flight (TOF) technique was employed in a similar manner to Mitsuda and Endoh [3] and Dokukin and co-workers [4] for studies of magnetization in polycrystalline ferromagnets.

2. Experiment

2.1. Samples

The ribbons (10 mm wide and 45 μm thick) were produced by planar flow casting of the melt of master alloy using a single-roller laboratory device of the Institute for Metals and Technology at the Bulgarian Academy of Sciences.

X-ray diffraction analyses were carried out for phase control and to prove the amorphousness of the samples. The actual chemical composition was determined by means of a Spectroflame spectrometer, Germany, which uses inductively coupled plasma.

0953-8984/93/509277+10$07.50

From macroscopic magnetic measurements the saturation magnetization ($B_S = 0.56$ T), coercive force ($H_C = 29.5$ A m^{-1}), and initial ($\mu^{in} = 1900$) and maximum ($\mu^{max} = 9500$) permeabilities were determined [5]. Such values are typical for the magnetic parameters of many Fe–Co-based amorphous ribbons well known as very soft magnetic materials [6]. Figure 1 illustrates the hysteresis loop of amorphous $Fe_{78}Co_{8.1}B_{13.9}$ ribbon.

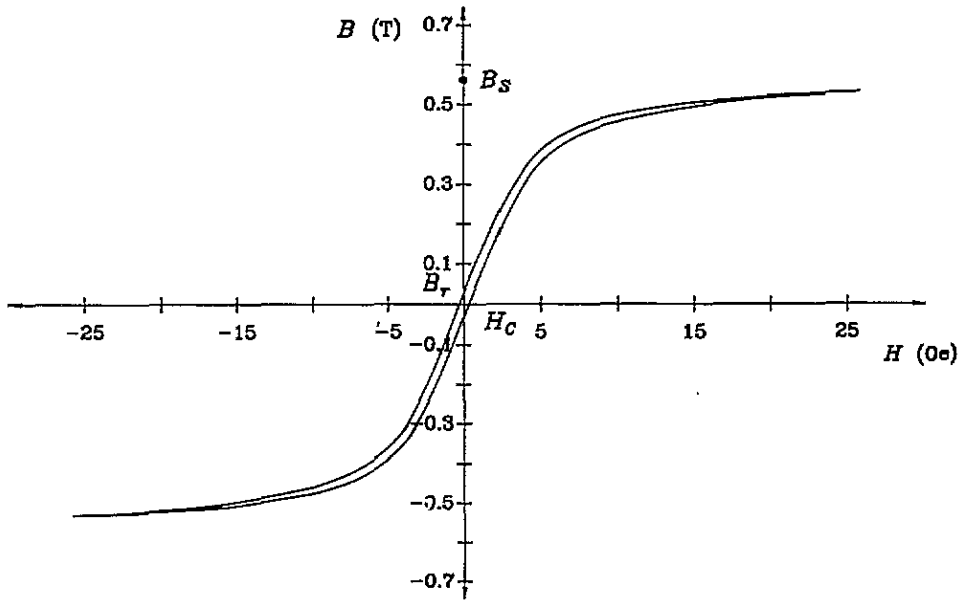

Figure 1. The hysteresis curve of amorphous ferromagnetic ribbon with composition $Fe_{78}Co_{8.1}B_{13.9}$.

The surface region in the central part of the ribbon in the vicinity of the ribbon axis was examined by regular optical methods. By means of a magnetic colloid fluid stripe domains (45–50 μm thick and 50–100 μm long) with the magnetization set at an acute angle of about 20° to the axis were visualized when a magnetic field H_{ext} was applied along the ribbon axis. The point of interest in the Bitter technique observations lies in the fact that variations in $|H_{ext}|$ from a value near saturation to one third of it do not lead to substantial changes in the mean domain spacing but the domains become shorter. On the other hand, mainly oval domains with an average size of 40–50 μm were observed by the polar Kerr effect in a field perpendicular to the ribbon surface.

2.2. *Neutron depolarization measurements*

The neutron depolarization experiment was performed at room temperature on stripes of ribbon 60 mm long. The SPN time-of-flight instrument on beam 8 of the IBR-2 pulsed reactor of JINR, Dubna [7] was used. The experimental arrangement is sketched in figure 2. A neutron flight-path of 36.77 m and a pulse duration of 300 μs were used. The cross section of the neutron beam was confined to 20 mm in height and 2 mm in width by cadmium diaphragms in order to irradiate the middle part of the sample under study. Figure 3 shows the experimental geometry.

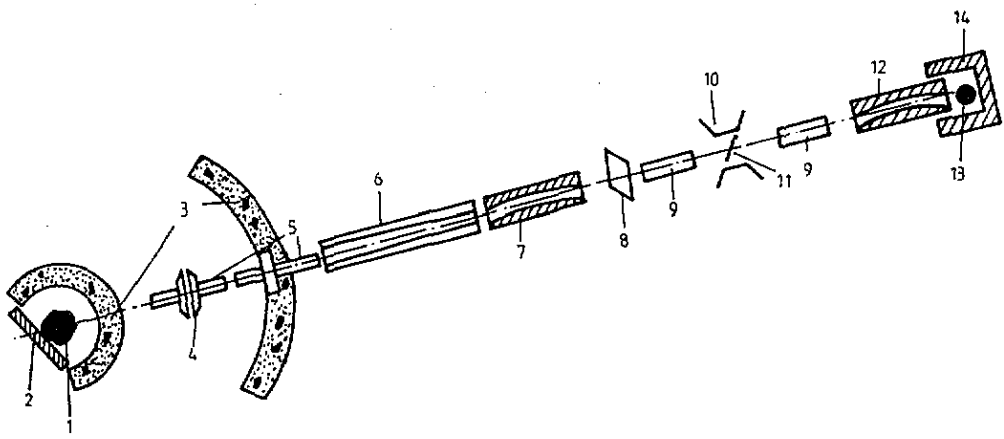

Figure 2. Arrangement for depolarization studies by means of the spectrometer for polarized neutrons, SPN, of JINR. 1: Reactor core. 2: Moderator. 3: Biological shielding. 4: Double-disc background-suppressing chopper. 5: Collimators. 6: Ni-coated conical mirror neutron guide. 7: Bent polarizing neutron guide. 8: Spin-flipper. 9: Mirror neutron guides. 10: Electromagnet. 11: Sample. 12: Bent analysing neutron guide. 13: ^{3}He neutron detector. 14: Neutron beam stop.

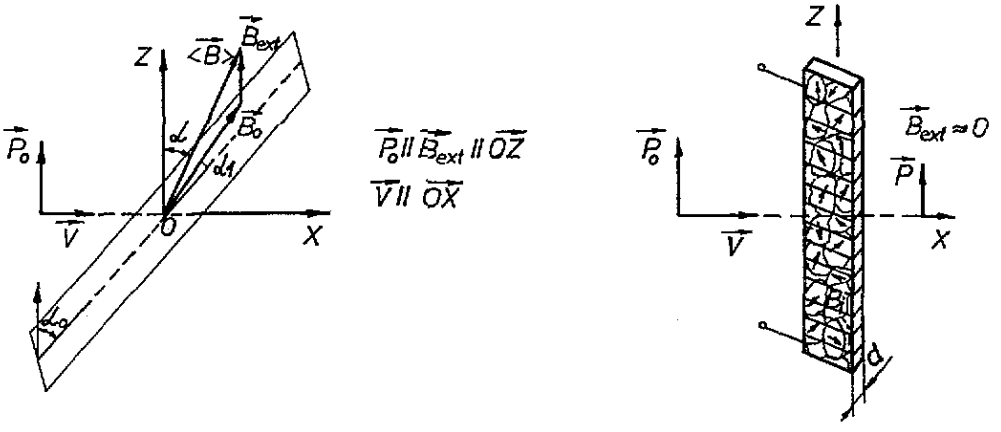

Figure 3. *Experimental geometry. Left: sample surface inclined under an angle* $\alpha_0 = 30°$ *with* respect to the z axis, $|B_{ext}| = 345$ G; right: $\alpha_0 = 0°$, $B_{ext} = 0$ G.

The mean polarization $|P_0|$ of incident neutrons with wavelengths from 0.09–0.4 nm was 94% or better. The polarization vector P_0 points to the vertical direction, defined as the z axis. The set-up allows an analysis of the z component of the transmitted polarization vector P. Therefore, by means of the TOF method, the wavelength dependence of the D_{zz} component of the depolarization matrix is measured. The depolarization coefficient $D = D_{zz}$ is determined from flipping ratio measurements using the expression

$$D = \left(\frac{1-R}{1+R}\right)_{\text{with sample}} \left[\left(\frac{1-R}{1+R}\right)_{\text{without sample}}\right]^{-1} \tag{1}$$

where $R = R(\lambda) = I_+(\lambda)/I_-(\lambda)$ is the ratio of the neutron count rate $I_+(\lambda)$ and $I_-(\lambda)$ recorded with flipper switched on and off, respectively.

The first set of measurements (see figure 3, right) was performed on a sample (a single stripe) centred in the polarized neutron beam inside a magnetizing coil and demagnetized in an alternate magnetic field with a gradually decreasing amplitude from 1600 A m^{-1} to zero. Next (figure 3, left) the sample was inclined so that the incident polarization vector P_0 made an angle $\alpha_0 = 30°$ with respect to the ribbon axis. The measurements were carried out in an external magnetic field of 345 G applied along the z axis. In order to reduce stray fields the sample ends were set in contact with the poles of the electromagnet. Figures 4 and 5 show the measured depolarization oscillation in dependence on the neutron wavelength. In fact, figure 4 displays the data obtained for a composite sample consisting of five stripes cut from the ribbon and piled together with the ejection axis kept parallel. The angular frequency of the oscillations was altered this way approximately by a factor of five (see below).

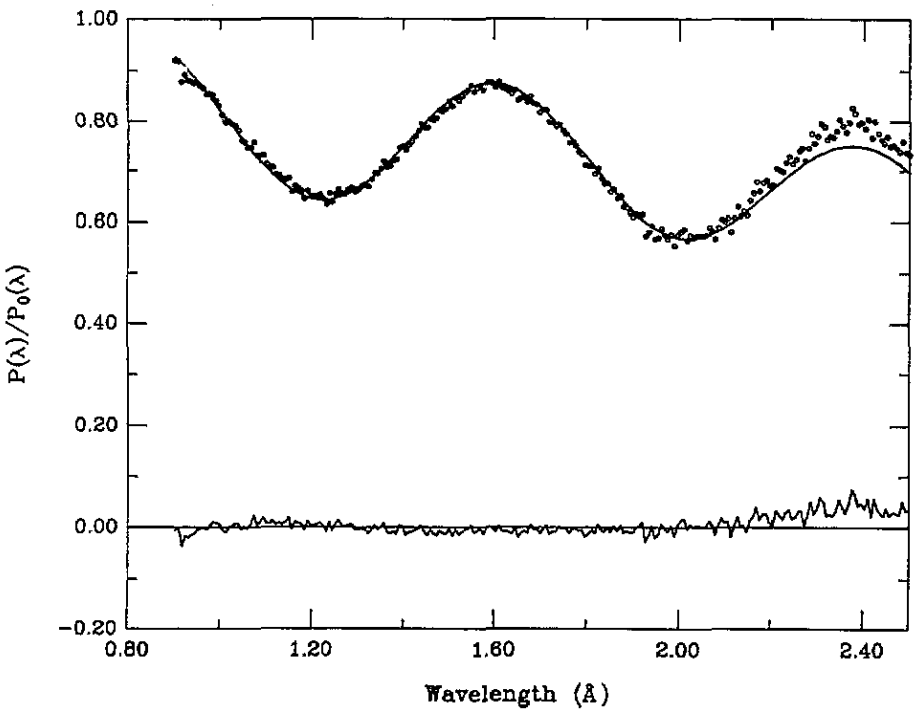

Figure 4. Oscillation of the depolarization coefficient D_{zz} (see text) against neutron wavelength measured for the sample $Fe_{78}Co_{8.1}B_{13.9}$ in an applied field (B_{ext} = 345 G). Points: measured intensities; full curve: calculated. The difference (measured minus calculated curve) is also shown. Best fit parameters: $\langle B \rangle = 6150 \pm 5$ G, $B_0 = 5834 \pm 6$ G, $\alpha = 23° 24' \pm 8'$, $\alpha_\perp = 5° 12' \pm 3'$, $\langle \Delta B \rangle = 176 \pm 20$ G, $(\langle \Delta B_\perp^2 \rangle/\delta)^{1/2} = 78.6 \pm 0.9$ G $\mu m^{-1/2}$. Reduced $\chi^2 = 1.15$.

3. Domain structure models

As was shown by Rosman and Rekveldt [8] recently, both classical [1,9] and quantum

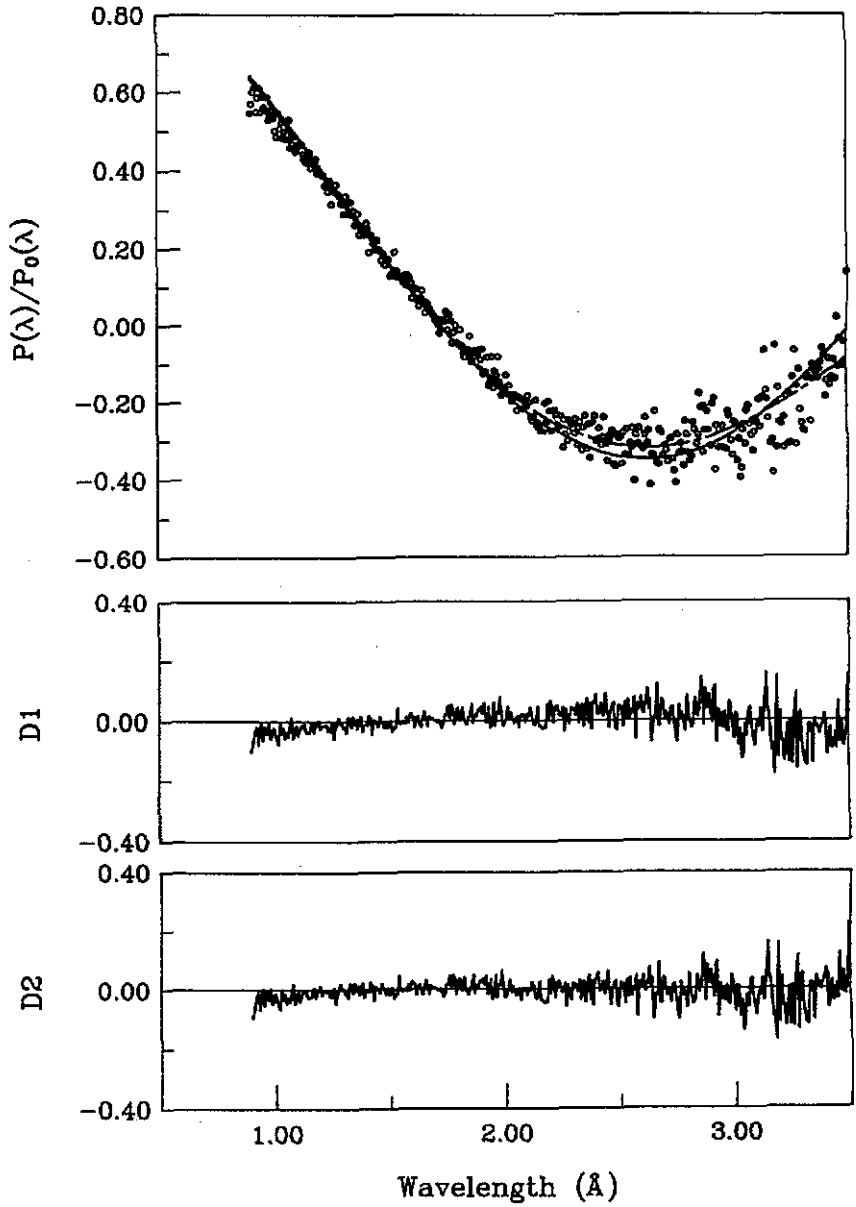

Figure 5. Wavelength dependence of the depolarization by the demagnetized sample $Fe_{78}Co_{8.1}B_{13.9}$ in a zero field. Points: measured intensities; curve: calculated. D_1 and D_2 are the difference (measured minus calculated) curves corresponding to the fit using the sandwich-like LL domains model: $\langle B \rangle = (6806 \pm 39)$ G, $\Delta\Theta/\delta' = (25.12 \pm 0.26) \times 10^{-3}$ rad μm^{-1} (dashed curve), reduced $\chi^2 = 0.84$; and the model of penetrating domains: $B_{av} = (5760 \pm 16)$ G, $\alpha = 167° 48' \pm 1° 48'$ (full curve), reduced $\chi^2 = 0.7$.

theoretical [10–12] (scattering) theories for a description of the phenomenon of neutron depolarization lead to formulae which are essentially the same. In terms of the pictorial classical approaches [1,9] the depolarization of transmitted polarized neutrons originates

from the uncorrelated precessions which the neutron magnetic moments make in the presence of magnetic inhomogeneities. The individual magnetic domain is a magnetic inhomogeneity in which induction is constant or remains of the same order of magnitude over a region with a certain size (domain size), δ, along the neutron trajectory.

For the general case of a mean local magnetic induction in the region traversed by the beam $\boldsymbol{B}_i$ acting under an angle α with respect to the incident polarization vector $\boldsymbol{P}_0$ it follows from simple geometric considerations that due to the Larmor rotation of the neutron spins by an angle φ the magnitude of polarization $|\boldsymbol{P}|$ is given by

$$|\boldsymbol{P}| = |\boldsymbol{P}_0|(\cos^2\alpha + \sin^2\alpha\cos\varphi) \tag{2}$$

with

$$\varphi = \gamma B_i t = C B_i \delta\lambda \tag{3}$$

where $\gamma = 1.83 \times 10^4\ \mathrm{G^{-1}\ s^{-1}}$ is the gyromagnetic ratio of the neutron, $t = \delta/v$ denotes the time of interaction, v is the neutron velocity, and the constant C is equal to 4.663×10^{-5} for B in G, δ in μm and λ in nm.

For multidomain ferromagnets both the classical and scattering theories predict that the logarithmic polarization is proportional to the square of the wavelength, i.e. $\ln[P(\lambda)/P_0] \sim -A_1\lambda^2$, or remains practically wavelength independent, $\ln[P(\lambda)/P_0] \sim -A$. The coefficient of proportionality is particularly simple in the framework of the classical description of Halpern and Holstein [9] in the following two limiting cases.

(i) Small precession ($m\pi \ll 1$, where m is the number of precessions)

$$A_1 \sim \langle \Delta B^2 \rangle \delta d_{\mathrm{eff}}. \tag{4}$$

(ii) Large precession ($m\pi \gg 1$)

$$A \sim \frac{\langle \Delta B^2 \rangle}{(\langle B \rangle)^2} \frac{d_{\mathrm{eff}}}{\delta}. \tag{5}$$

For a ferromagnet near saturation, which is the case of figure 3 (left), local magnetic induction can be expressed as

$$\boldsymbol{B}(t) = \langle \boldsymbol{B} \rangle + \Delta\boldsymbol{B}_{\parallel}(t) + \Delta\boldsymbol{B}_{\perp}(t) \tag{6}$$

where $\langle \boldsymbol{B} \rangle$ is the mean magnetic induction of the sample and the quantities $\Delta\boldsymbol{B}_{\parallel}$ and $\Delta\boldsymbol{B}_{\perp}$ denote the parallel and perpendicular deviations of $\boldsymbol{B}$ from $\langle \boldsymbol{B} \rangle$. Both components of the deviation $\Delta\boldsymbol{B}$ are expected to be small, since $|\Delta\boldsymbol{B}| \ll |\boldsymbol{B}|$, but as shown by theory [9–11], they cause a decrease in the degree of polarization.

The concrete form of the constant A_1 for a ferromagnet near saturation is given by [9]

$$A_1 = \tfrac{1}{2} C^2 \langle B_{\perp}^2 \rangle \langle \delta \rangle d_{\mathrm{eff}} \tag{7}$$

where $\langle B_{\perp}^2 \rangle$ is the mean squared perpendicular component of $\langle \boldsymbol{B} \rangle$ and d_{eff} is the effective sample thickness along the neutron path.

For the experimental geometry described in figure 3 (left), expression (2) has to be modified in order to account for the expected variation of the mean induction within small limits $\pm\langle\Delta B\rangle/2$ across the cross section of the beam. Integrating (2) gives

$$P(\lambda) = \frac{1}{\langle\Delta B\rangle}\int_{\langle B\rangle-\langle\Delta B\rangle/2}^{\langle B\rangle+\langle\Delta B\rangle/2} P_0 e^{-A_1\lambda^2}\left[(\cos^2\alpha + \sin^2\alpha\cos(B\delta\lambda C)\right] dB$$

$$= P_0 e^{-A_1\lambda^2}\left(\cos^2\alpha + 2\sin^2\alpha\frac{\sin x}{x}\cos(C\delta\lambda\langle B\rangle)\right) \tag{8}$$

where $x = (\langle\Delta B\rangle\delta\lambda C)/2$. Moreover, the validity of the small-precession limit was presumed.

Making use of the presumption that $\langle\Delta B\rangle/\langle B\rangle \ll 1$, and taking only the first two terms in the expansion of $\sin x/x$, one comes to the final expression

$$P(\lambda)/P_0(\lambda) = e^{-A_1\lambda^2}\cos^2\alpha + e^{-A_2\lambda^2}\sin^2\alpha\frac{\cos(\omega_\lambda\lambda - \tan^{-1}\omega_0\tau_0)}{\sqrt{(\omega_0\tau_0)^2+1}}$$

or

$$P(\lambda)/P_0(\lambda) = e^{-A}\left(\cos^2\alpha + e^{-A_3\lambda^2}\sin^2\alpha\frac{\cos(\omega_\lambda\lambda - \tan^{-1}\omega_0\tau_0)}{\sqrt{(\omega_0\tau_0)^2+1}}\right) \tag{9}$$

where the term $\tan^{-1}\omega_0\tau_0$ appears with $\omega_0 = \gamma\langle B\rangle d/L$ and the total flight path, L, is in metres. This term describes the phase shift due to the uncertainty in the precession angle caused by the actual width (FWHM) of neutron pulses τ_0. It is assumed that the burst of reactor power is smeared in time according to an exponential law. In our case this correction term is practically negligible because $\tau_0 \approx 3\times10^{-4}$ s and the ratio of the sample thickness to the neutron flight-path is also very small, $d/L \approx 10^{-6}$, so that $\tan^{-1}\omega_0\tau_0 \ll 1$ and $\sqrt{(\omega_0\tau_0)^2+1} \approx 1$.

Here the explicit form of the quantities A, A_1, A_2, and A_3 reflects the domain model in a given magnetization state and depends on the magnitude of the angle of polarization vector precession within a domain.

The angular frequency of measured oscillation of depolarization on the λ scale is $\omega_\lambda = C\langle B\rangle d_{\text{eff}}$, where $d_{\text{eff}} = d/\cos\alpha_0$ is the effective sample thickness along the neutron path, α_0 is the angle between the sample surface and the direction of the external field $\boldsymbol{B}_{\text{ext}}$, $\langle\boldsymbol{B}\rangle$ is expressed as $\langle\boldsymbol{B}\rangle = \boldsymbol{B}_0 + \boldsymbol{B}_{\text{ext}}$, and $\boldsymbol{B}_0$ is the saturation induction.

A simple model of magnetic domains penetrating the bulk was adopted in considering the results for depolarization by the sample in an unmagnetized ferromagnetic state, which are displayed in figure 5. The relevant formulae are derived below.

The domain size is several orders of magnitude larger than the neutron wavelength λ. Therefore, we could assume that a portion of neutrons of a given λ pass through the ith domain under an angle α_i with respect to the domain induction $\boldsymbol{B}_i$. All local $|\boldsymbol{B}_i|$ are expected to be equal to each other and almost equal to the saturation induction $|\boldsymbol{B}_s|$. Then (2) should be regarded as describing the neutron passage through an individual domain. This assumption allows one to use integration over the projections of polarization on the local induction direction $d\cos\alpha_i$, where α_i runs from zero to a certain maximum angle α. The angle α is a measure for the deviation of the individual domain induction vectors from the direction of incident polarization $\boldsymbol{P}_0$ (z axis). If one also takes into account the small

variation in ribbon thickness, which is typical for the amorphous ribbons obtained by planar flow casting, the integration can be written

$$P(\lambda) = \frac{1}{\cos\alpha - 1}\frac{1}{\Delta d}\int_1^{\cos\alpha}\int_{d-\frac{\Delta d}{2}}^{d+\frac{\Delta d}{2}} P(\lambda, \alpha', d')\,\mathrm{d}\cos\alpha'\,\mathrm{d}d'. \tag{10}$$

Here a uniform distribution of $\cos\alpha$ in the interval $[1, \cos\alpha]$ and of thickness d in the interval $[d - \frac{\Delta d}{2}, d + \frac{\Delta d}{2}]$ is supposed. The integration is straightforward:

$$D_{zz} = \frac{1 - \cos^3\alpha}{3(1 - \cos\alpha)} + \frac{2 - \cos\alpha(3 - \cos^2\alpha)}{3(1 - \cos\alpha)}\cos\Phi_\lambda \frac{\sin C B_{\mathrm{av}} \frac{1}{2}\Delta d\lambda}{C B_{\mathrm{av}} \frac{1}{2}\Delta d\lambda} \tag{11}$$

where $\Phi_\lambda = C B_{\mathrm{av}} d\lambda$ is the angle of neutron spin precession within a domain, and Δd is the uncertainty in sample thickness d, or in domain size, respectively.

Our experimental results have also been considered in terms of domain structure models analysed by other authors.

For the D_{zz} depolarization component [1, 3]

$$D_{zz} = \left[1 - (1 - \cos\Phi_\lambda)\left(1 - \frac{\langle B_z^2\rangle}{\langle B\rangle^2}\right)\right]^{d/\langle\delta\rangle} \tag{12}$$

where $\Phi_\lambda = C\langle B\rangle\langle\delta\rangle\lambda$ is the net rotation angle of the neutron spin within a single magnetic domain of average size $\langle\delta\rangle$ along the neutron flight-path, d is the sample thickness, and λ is the neutron wavelength.

The formula (12) is derived for a model of a specimen magnetized along the z axis (B_z = constant $\neq 0$) for which the other two components of magnetization remain uncorrelated, i.e. B_x and B_y are randomly distributed in the plane perpendicular to the z direction. The z component of magnetic domain induction may originate from an applied magnetic field or the presence of a single-axis magnetic anisotropy.

For a sandwich-like domain structure of Landau–Lifshitz type, with closure domains at opposite faces of the specimen magnetized either parallel or antiparallel, Kraan and Rekveldt [13] have derived

$$D_{zz} \approx \tfrac{2}{3}(\Delta\Theta)\frac{d}{\delta'}\left(\frac{\sin\Phi_\lambda}{\Phi_\lambda} - \cos\Phi_\lambda\right) + \cos\Phi_\lambda \tag{13}$$

where $\Delta\Theta$ is a parameter describing the disorientation of main domains and δ' is the closure domain height. This model is considered in detail elsewhere [14].

A least-squares fitting procedure was written in order to test the validity of the assumed models. The conventional χ^2 factor was used as one of the possible criteria for goodness-of-fit.

4. Results and discussion

In figures 4 and 5 the experimental values are represented by points, and the curves represent the results of the fitting procedure using (9), (11), and (13) with the parameters as given in the caption to the figure. The magnitude of saturation magnetization B_s measured by means of a magnetometer is lower by about 4% than the estimate B_0 determined from the

depolarization oscillation curve shown in figure 4. The calculated value of the angle α_1 between $\boldsymbol{B}_0$ and the sample surface, $\alpha_1 = 5° 12'$, implies that in the state of complete saturation the sample magnetic induction is oriented slightly out of the sample surface. This means that there is a magnetic anisotropy whose axis essentially lies in the ribbon plane and a small contribution of a term perpendicular to the surface. Such a result could be expected in view of the findings of Kronmüller [15] and his collaborators [16, 17], and another author [6], for the domain structure in amorphous ribbons fabricated by planar flow casting.

The attempt to fit (12) to the experimental data in figure 5 led to results which are in contradiction with the fact that the sample had been carefully demagnetized. First runs with $\langle B \rangle$ and B_z varied within broad limits ($4000 < \langle B \rangle < 7000$ G and $0 < B_z < 1000$ G) failed (reduced $\chi^2 > 50$). The next runs, with no restricting intervals, were successful. However, despite the reasonable values of χ^2 (of the order of 0.7–0.9) achieved for both $d = \delta$ and $d \neq \delta$, the estimates of $\langle B \rangle$ of about 6020 G and of B_z of about 3400 G imply the presence of too large a z component of the magnetic induction, which disagrees with the observations.

The sandwich-like model gave a better fit, which was further improved slightly by the model of penetrating domains (figure 5). In fact, these two models cannot be safely distinguished on the basis of the χ^2 criterion only, since they yielded nearly the same value of χ^2. However, the penetrating domains model gave a value of the mean induction $\langle B \rangle = B_{av} = 5760$ G which is more reasonable than the estimate $\langle B \rangle = 6806$ G from the fit corresponding to the sandwich-like model, both compared with the estimate $\langle B \rangle = B_0 = 5834$ G from the angular frequency of the oscillation curve of neutron depolarization, taken as a reference. This last value is in good agreement with the results from magnetization measurements, $B_s = 5600$ G. The small difference of only 74 G can be explained with the inhomogeneity of the mean induction, $\langle B \rangle$, estimated to be $\langle \Delta B \rangle = 176$ G. In addition, it is interesting to note that from the domain structure found it follows that, in the demagnetized state, the sample was seemingly not demagnetized completely since the maximum angle α between the local B_i and the ribbon axis is estimated to be $\alpha = 168°$, i.e. it remains lower than $\alpha = 180°$ which should correspond to orientations of local magnetic inductions of individual domains fully at random.

In conclusion, we feel we have demonstrated that by using wavelength-dependent depolarization measurements some important magnetic domain quantities can be determined, such as the magnitude and direction of mean magnetization, the mean domain size, the magnetization fluctuations and, under favourable circumstances, the local magnetic induction within a single domain and domain disorientation. In some sense it is the same information obtained by the three-dimensional depolarization technique, which is convenient for steady-state reactors, but the combination of the neutron time-of-flight method with pulsed neutron sources opens up a new area for the research in the field.

Acknowledgments

We wish to thank Professor O Schärpf (ILL) for helpful discussions, and Dr Chernenko (JINR), Mr V Tcvetkov (INRNE) and Dr Christemov (IMT) for help in some of the measurements. The financial support of the National Fund for Scientific Research of Bulgaria is gratefully acknowledged.

References

[1] Rekveldt M Th 1973 *Z. Phys.* **259** 391; 1989 *Textures Microstruct.* **11** 127
[2] Dobrzynski L and Rekveldt M 1991 *J. Magn. Magn. Mater.* **94** 153
[3] Mitsuda S and Endoh Y 1985 *J. Phys. Soc. Japan* **54** 1570
[4] Dokukin E, Korneev D, Loebner W, Pasjuk V, Petrenko A and Rzany H 1988 *J. Physique Coll.* **49** C8 2073
[5] Krezhov K and Lilkov V 1993 *Proc. 7th ISCMP (Varna, 1993)* (Singapore: World Scientific)
[6] Zolotukhin J V 1986 *Physical Properties of Amorphous Metallic Materials* (Moscow: Metallurgiya)
[7] Ostanevich Ju M *et al* 1985 *JINR Preprint* R-85-310, Dubna
Taran Yu V (ed) 1992 Neutron experimental facilities at JINR *User's Guide*
[8] Rosman R and Rekveldt M Th 1990 *Z. Phys.* B **79** 61
[9] Halpern O and Holstein T 1941 *Phys. Rev.* **59** 960
[10] Maleev S and Ruban V 1970 *Sov. Phys.–JETP* **31** 111
[11] Toperverg B and Weniger T 1989 *Z. Phys.* B **74** 105
[12] Sbitnev V I 1989 *Z. Phys.* B **74** 321
[13] Kraan W and Rekveldt M 1978 *J. Magn. Magn. Mater.* **8** 168
[14] Stüsser N, Builtjes J H and Rekveldt M Th 1987 *J. Magn. Magn. Mater.* **67** 207
[15] Kronmüller H 1983 *Phil. Mag.* B **48** 125; 1985 *Phys. Status Solidi* b **127** 531
[16] Kronmüller H and Gröger B 1981 *J. Physique* **42** 1285
[17] Fernengel W and Kronmüller H 1983 *J. Magn. Magn. Mater.* **37** 167